

# Coupled reaction channel analysis for proton transfer in $^{116}\text{Sn}+^{60}\text{Ni}$

Chandra Kumar<sup>1,\*</sup> and S. Nath<sup>1</sup>

<sup>1</sup>Inter-University Accelerator Centre, Aruna Asaf Ali Marg, New Delhi 110067, India

**Abstract.** We carried out exact finite-range coupled reaction channel analysis for one- and two-proton stripping channels in the collision  $^{116}\text{Sn}+^{60}\text{Ni}$ , based on a parameter free double-folding potential. Large-scale shell model calculations were performed for obtaining spectroscopic amplitudes for projectile and target overlaps. Transition between the ground states was found to contribute the maximum to the one-proton stripping cross sections. Data for two-proton stripping were significantly underpredicted by the successive and the microscopic cluster transfer mechanisms. The extreme cluster model for the transfer of a pair of nucleons was successful in reproducing the data for two-proton stripping channel. No arbitrary scaling of the cross sections had to be invoked in our analysis. Information on individual transitions, inclusion of additional states in the intermediate partition and more realistic shell model calculations may further refine our results.

## 1 Introduction

Heavy ion-induced multi-nucleon transfer (MNT) reactions [1] are important for studying the transition from quasielastic to deep-inelastic regime [2], production of heavy neutron rich nuclei [3, 4] and probing nucleon-nucleon correlation [5, 6]. MNT reactions are of significant interest in the study of neutrinoless double  $\beta$ -decay through heavy ion double charge exchange reactions [7]. MNT channels are also known to influence fusion dynamics [8] near and below the Coulomb barrier.

In recent years, a substantial amount of work, both theoretical and experimental, on heavy ion-induced MNT reactions in intermediate and heavy mass systems has been reported. However, a relatively smaller body of work exists on proton transfer channels at near barrier energies compared to the same on neutron transfer channels. The importance of the various degrees of freedom involved in the reaction mechanism can be studied by comparing the experimental data with theory, which incorporates both nuclear structure and dynamics information. Many authors had in the past (see *e.g.*, Ref. [9]) pointed to the difficulty in theoretically reproducing measured MNT cross sections.

Along with the availability of precision data on heavy ion-induced MNT cross sections, significant progress has also been made in the theoretical front lately. Microscopic description of MNT processes without recourse to arbitrary normalization factors has been reported for many systems (see *e.g.*, Ref. [10–12]). However, ambiguities still exist in the quantum-mechanical treatment of MNT observables, especially in the choice of potential parameters, nuclear structure inputs and states of participating nuclei to be coupled for a given channel [13].

Evidence of proton-proton correlations has recently been reported in the system  $^{116}\text{Sn}+^{60}\text{Ni}$  [5]. This system is characterized by closed proton and open neutron shells and the measurement was carried out at sub-barrier energies to ensure negligible nuclear effects. Measured transfer probabilities ( $P_{tr}$ ) for one-proton ( $1p$ ) and two-proton ( $2p$ ) transfer were compared with semiclassical calculations. The authors justified the application of the semiclassical theory [14] based on the fact that the wavelength associated with the relative motion in this heavy ion-induced collision was considerably shorter than the interaction region. While experimental  $P_{tr}$  for the  $1p$ -channel was fairly well reproduced by the calculation, the same for the  $2p$ -channel had to be scaled down by a large factor to match with the theory. The authors attributed the mismatch to strong proton-proton correlations that were not taken into account in the calculations, which considered only successive transfer mechanism.

Here, we report the analysis of  $1p$ - and  $2p$ -transfer in  $^{116}\text{Sn}+^{60}\text{Ni}$  by exact finite range coupled reaction channel (CRC) calculations [15] employing a parameter free double-folding optical potential [16].

## 2 Shell-Model calculations

Spectroscopic amplitude ( $S$ ) is an essential ingredient for CRC calculations. The  $S$ s for one- and two-proton transfer in  $^{116}\text{Sn}+^{60}\text{Ni}$  have either been obtained from the literature (if available) or been extracted from large-scale shell model calculations using the code `KSHELL` [17].

For the heavier (*i.e.*,  $^{116}\text{Sn}$ ,  $^{117}\text{Sb}$  and  $^{118}\text{Te}$ ) nuclei, two different interactions, *viz.*, the `SN100PN` [18, 19] and the monopole-optimized effective [20] interactions have been incorporated in shell model calculations. In both the cases, a model space has been used in which the  $^{100}\text{Sn}$  nu-

\*e-mail: [dwngn10chandra@gmail.com](mailto:dwngn10chandra@gmail.com)

cleus served as the core, with  $1g_{7/2}$ ,  $2d_{5/2}$ ,  $2d_{3/2}$ ,  $3s_{1/2}$  and  $1h_{11/2}$  as the valence orbits for both neutrons and protons. While extracting the wave functions for  $^{116}\text{Sn}$ , we did not impose any truncation on the model space.  $^{118}\text{Te}$  being a mid-shell nucleus, the dimension of the model space became very large. Because of computational challenges, we imposed some truncations on the model space in this case. Specifically, the maximum number of neutron excitations in the  $1h_{11/2}$  orbit was limited to 2. Both the minimum and the maximum occupation numbers of valence protons in the  $1h_{11/2}$  orbit were restricted to 0. The numbers of valence particles in other orbits were unconstrained. The wave functions of  $^{117}\text{Sb}$  were generated using a truncation method similar to that used in Ref. [21], employing the SN100PN interaction. However, for the monopole-effective interaction, we utilized a truncation scheme similar to that applied for  $^{118}\text{Te}$ .

The wave functions for the lighter (*i.e.*,  $^{60}\text{Ni}$ ,  $^{59}\text{Co}$  and  $^{58}\text{Fe}$ ) nuclei were generated using two distinct interactions and the corresponding model spaces. These interactions, *viz.*,  $\text{kb3g}$  [23] and  $\text{fpd6npn}$  [24], were employed within the  $\text{fp}$  model space which consisted of  $1f_{7/2}$ ,  $2p_{3/2}$ ,  $1f_{5/2}$ , and  $2p_{1/2}$  valence orbits for both neutrons and protons.  $^{40}\text{Ca}$  was considered the core and the minimum and the maximum numbers of occupation for neutrons in  $1f_{7/2}$  orbit, due to computational constraints, were limited to 8 in both the cases. No truncation was imposed on other valence orbits.

Reasonably good matching between the experimental and the theoretical energy spectra was achieved for all these nuclei, though, the values of  $S$  for projectile overlaps differed (Table 1).

### 3 Coupled reaction channel calculations

Exact finite-range CRC calculations were carried out to investigate the microscopic mechanism of  $1p$ - and  $2p$ -stripping in the collision  $^{116}\text{Sn}+^{60}\text{Ni}$  [5] below the Coulomb barrier, using the code `FRESCO` [15, 25]. The double-folding São Paulo potential, generated by the code `REGINA` [26], was employed in the real and the imaginary parts of the optical potential in each partition. The strength coefficients for the real and the imaginary parts of the potential were taken as 1.0 and 0.6, respectively. The required Coulomb matrix element as well as the nuclear deformation length were obtained from the literature [27, 28]. The Woods-Saxon form was assumed for the binding potential in order to generate the bound state wave functions for the single proton and the pair of protons with respect to the respective cores.

In case of one-step transfer, the depth was adjusted to mimic the experimental separation energies for one and two proton(s). On the other hand, for two-step transfer, the depth was varied to reproduce the experimental separation energy in each step. The reduced radii and diffuseness parameters were, respectively, 1.30 fm and 0.7 fm in all cases. The transfer matrix-elements were generated using prior representation of the potential with the inclusion of complex remnant terms, for the one-step transfer. The

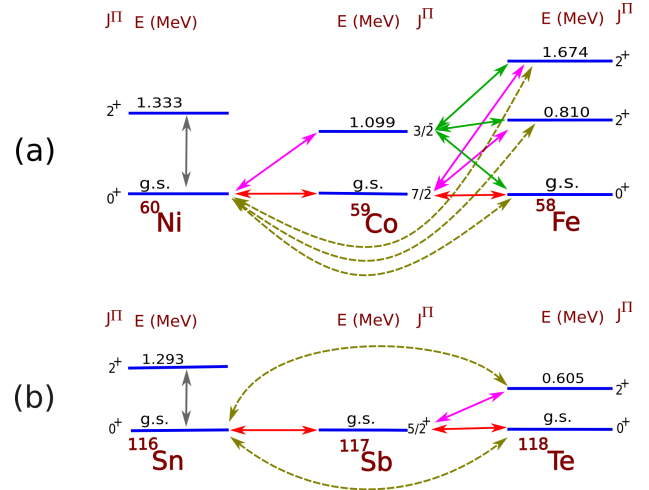


Figure 1: Coupling schemes for (a) the target and (b) the projectile overlaps considered in the CRC calculations for the reactions  $^{60}\text{Ni}(^{116}\text{Sn}, ^{117}\text{Sb})^{59}\text{Co}$  and  $^{60}\text{Ni}(^{116}\text{Sn}, ^{118}\text{Te})^{58}\text{Fe}$ . The solid lines represent transitions in the two-step mechanism while the dashed lines correspond to transitions in the one-step mechanism.

two-step transfer was investigated in the prior-post representation of the transition potential to minimize the effects of the non-orthogonal terms [15].

Two different mechanisms were considered for the transfer of a pair of protons. In the two-step mechanism, the two protons were transferred, successively, through an intermediate partition. Conversely in the one-step mechanism, the interaction potential was considered to act on the centre of mass of the correlated proton pair. Under this assumption, the pair transfer can be viewed as a single quasi-particle transfer mechanism. In the first approach within the single-step mechanism, the so-called microscopic cluster model approach, the ‘di-proton’ cluster was assumed to be either in the  $1s$  ( $n = 1, l = 0$ ) or in the  $1p$  ( $n = 1, l = 0$ ) internal state with respect to the core, with the intrinsic spin  $S = 0$  (anti-parallel configuration) or  $S = 1$  (parallel configuration), respectively. Details about the procedure followed for calculation of  $S$ s for cluster transfer can be found elsewhere [13]. In the second approach of single-step mechanism, within the framework of the extreme cluster model, the proton-pair was constrained to be in the  $1s$  internal state. Here, the  $S$ s for both projectile and target overlaps were, customarily, assigned the value of 1.0. In this theoretical study, differential cross sections for  $1p$  and  $2p$ -stripping were computed first, as a function of the distance of closest approach ( $D$ ) for a Coulomb trajectory, defined by  $D = \frac{1.44Z_p Z_t}{2E_{c.m.}} \left[ 1 + \text{cosec} \left( \frac{\theta_{c.m.}}{2} \right) \right]$ . Here,  $Z_p, Z_t$  are respectively the atomic charges of the projectile and the target,  $E_{c.m.}$  is the energy available in the centre of mass (c.m.) frame of reference and  $\theta_{c.m.}$  is the scattering angle in the c.m. frame. Cross sections were further converted to  $P_{tr}$  adopting the norm followed for experimental data [5].

Coupling scheme considered in the CRC calculations is shown in Fig. 1.

Table 1: One-proton  $S$  relevant to the projectile overlaps. Results of shell model calculations and values available in the literature [22] are tabulated. Here  $n$ ,  $l$  and  $j$  are the principle quantum number, the orbital angular momentum and the total angular momentum of the proton, respectively.

| Initial state                        | $nl_j$     | Final state                            | Experimental    | SN100PN | Monopole |
|--------------------------------------|------------|--|-----------------|---------|----------|
| $^{116}\text{Sn}_{\text{g.s.}}(0^+)$ | $2d_{5/2}$ | $^{117}\text{Sb}_{\text{g.s.}}(5/2^+)$ | $0.95 \pm 0.07$ | -0.0968 | -0.5762  |
|                                      | $1g_{7/2}$ | $^{117}\text{Sb}_{0.527}(7/2^+)$       | $0.84 \pm 0.08$ | 0.0991  | 0.3883   |
|                                      | $3s_{1/2}$ | $^{117}\text{Sb}_{0.719}(1/2^+)$       | $0.71 \pm 0.06$ | 0.0537  | -0.5035  |

### 3.1 One-proton transfer

Results of CRC calculations for the reaction  $^{60}\text{Ni}(^{116}\text{Sn}, ^{117}\text{Sb})^{59}\text{Co}$  are shown in Fig. 2. Calculations were first carried out using  $S_s$  for  $1p$ -stripping from shell model calculations, based on SN100PN and monopole-optimized effective interactions. Both sets of calculations underpredicted measured data. Next we incorporated experimental  $S_s$  from the literature [22, 29] in the CRC calculations, which yielded results with satisfactory matching with measured data.

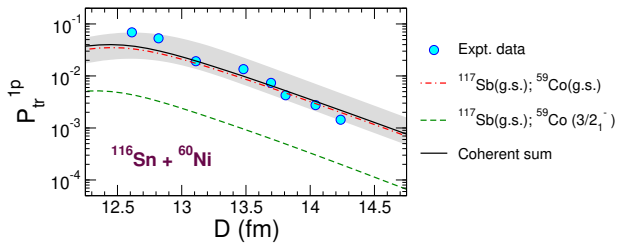


Figure 2: comparison between the experimental and theoretical transfer probabilities for the reaction  $^{60}\text{Ni}(^{116}\text{Sn}, ^{117}\text{Sb})^{59}\text{Co}$ . The shaded region denotes the uncertainty in calculated transfer probability caused by a variation of  $\pm 15\%$  in the spectroscopic amplitudes, used in CRC calculations.

It is evident from Fig. 2 that the ground state (g.s.) to g.s. transition contributes the most in measured cross sections. We further studied the contributions of the excited states of both collision partners. Inclusion of the first  $\frac{3}{2}^-$  state of  $^{59}\text{Co}$  caused marginal enhancement of the coherent sum. On the other hand, inclusion of the first excited state of  $^{117}\text{Sb}$  led to overestimation of experimental data. The importance of the g.s. to g.s. transition in case of  $1p$ -stripping channel was also pointed out by the authors of Ref. [5]. The total kinetic energy loss (TKEL) spectra for  $1p$ -stripping were found to peak near the g.s. to g.s.  $Q$ -value.

Large uncertainties are usually associated with measured  $S$ . To assess the impact of uncertainty in  $S$  on calculated  $P_{\text{tr}}$ , we varied the  $S_s$ , incorporated in CRC calculations by  $\pm 15\%$ . The shaded region in Fig. 2 shows the extent up to which calculated  $P_{\text{tr}}$  might vary. One may note that, all the data points lie within the range of calculated  $P_{\text{tr}}$ , caused by  $\pm 15\%$  uncertainty in  $S$ .

### 3.2 Two-proton transfer

Transfer of a pair of nucleons can proceed either by one-step or two-step process. Results of our calculations for  $P_{\text{tr}}$  for the reaction  $^{60}\text{Ni}(^{116}\text{Sn}, ^{118}\text{Te})^{58}\text{Fe}$  are shown in Fig. 3. In the case of sequential transfer, two protons are transferred one by one passing through the intermediate partition  $^{117}\text{Sb}+^{59}\text{Co}$ , populated through  $1p$ -transfer. We used here the same reduced binding radii and diffuseness parameters as in case of  $1p$ -transfer channel. The results underpredicted the experimental data by more than an order of magnitude. This discrepancy indicated that the two-step process was unlikely to be the preferred mode of transfer for this system. Next the microscopic cluster model calculations were performed with  $S_s$ , obtained from the shell model calculations. The results for the microscopic cluster model were lower by almost an order of magnitude in comparison with the same for sequential transfer. Finally, we carried out the extreme cluster model calculations, in which  $S_s$  for the cluster were taken as unity in all the transitions. The theoretical  $P_{\text{tr}}$  matched very well with the experimental data. The results indicated that the inelastic transition to the  $2_1^+$  state of  $^{118}\text{Te}$  in the final partition contributed significantly to measured  $P_{\text{tr}}$ .

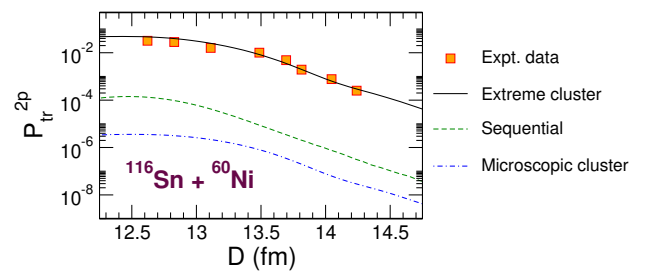


Figure 3: Comparison between the experimental and the theoretical transfer probabilities for the reaction  $^{60}\text{Ni}(^{116}\text{Sn}, ^{118}\text{Te})^{58}\text{Fe}$ . See text for details.

It is important to note the probable limitations in the results presented here. The ambiguities in the choice of states of the colliding nuclei in the calculations can be minimized if the individual transitions and population pattern of transfer products are experimentally verified. More states, allowed by angular momentum coupling, in the intermediate partition in case of  $2p$ -stripping could be considered, if adequate computational resources were available. Lastly, discrepancy between experimental and theoretical values of energies and limitation of the model space

used in shell model calculations might also cause the underestimation of experimental  $2p$   $P_{tr}$  by sequential and microscopic cluster approaches in CRC calculations. These aspects require further investigation. However, our study demonstrated that microscopic description of MNT mechanism in collision between two heavy ions, with no requirement for arbitrary normalization of the cross sections, is quite feasible within the CRC framework.

## 4 Conclusions

The mechanism of  $1p$ - and  $2p$ -stripping reactions in the  $^{116}\text{Ni}+^{60}\text{Ni}$  collision was studied within the exact finite-range CRC framework. The double-folding São Paulo potential was used for the entrance, intermediate and exit partitions.  $S$ s for the projectile and target overlaps, for both  $1p$  and  $2p$ -stripping channels, were obtained either from the literature or from large-scale shell model calculations. For the reaction  $^{60}\text{Ni}(^{116}\text{Sn}, ^{117}\text{Sb})^{59}\text{Co}$ , major contribution to transfer cross sections came from the g.s. to g.s. transition. Further, impact of coupling with the inelastic states in the exit partition was also investigated. The experimental  $S$ , used in the calculation, was varied to assess the effect of uncertainties in  $S$  on the transfer cross sections. It was found that  $\pm 15\%$  variation of  $S$  accommodated all the experimental data points. In the case of  $^{60}\text{Ni}(^{116}\text{Sn}, ^{118}\text{Te})^{58}\text{Fe}$ , we considered both sequential and simultaneous mode of transfer of a pair of protons within the CRC formalism. Further, two distinct approaches, *viz.*, microscopic cluster and extreme cluster models were employed for the one-step mechanism. It was found that two-step transfer and the microscopic cluster transfer mechanisms were significantly inadequate to describe experimental  $P_{tr}$  for  $2p$ -stripping. The measured  $P_{tr}$  was successfully reproduced by the extreme cluster model over the whole range of  $D$  explored in the experiment. One may, however, note that these results are susceptible to uncertainties originating from the lack of experimental corroboration for the transitions included in the calculation and limitations in shell model calculations. Encouraged by the results for proton-stripping channels, we are carrying out CRC analysis for neutron-pickup channels in  $^{116}\text{Sn}+^{60}\text{Ni}$  [6, 30], which will be reported elsewhere.

## Acknowledgements

One of the authors (C.K.) acknowledges financial support from the Council of Scientific and Industrial Research (CSIR), New Delhi via grant no. CSIR/09/760(0038)/2019-EMR-I. The authors acknowledge the National Supercomputing Mission (NSM) for

providing computing resources of 'PARAM Ganga' at the Indian Institute of Technology Roorkee, which is implemented by C-DAC and supported by the Ministry of Electronics and Information Technology (MeitY) and Department of Science and Technology (DST), Government of India, for carrying out large-scale shell model and coupled reaction channel calculations.

## References

- [1] L. Corradi, G. Pollarolo, and S. Szilner, *J. Phys. G: Nucl. Part. Phys.* **36**, 113101 (2009).
- [2] J. Diklić *et al.*, *Phys. Rev. C* **107**, 014619 (2023).
- [3] S. Heinz and H. M. Devaraja, *Eur. Phys. J. A* **58**, 114 (2022).
- [4] H. M. Devaraja, A. V. Yeremin, S. Heinz *et al.*, *Phys. Part. Nucl. Lett.* **19**, 693 (2022).
- [5] L. Corradi *et al.*, *Phys. Lett. B* **834**, 137477 (2022).
- [6] D. Montanari *et al.*, *Phys. Rev. Lett.* **113**, 052501 (2014).
- [7] F. Cappuzzello *et al.*, *Prog. Part. Nucl. Phys.* **128**, 103999 (2023).
- [8] Rudra N. Sahoo *et al.*, *Phys. Rev. C* **102**, 024615 (2020).
- [9] K. E. Rehm *et al.*, *Z. Phys. A* **340**, 281 (1991).
- [10] M Cavallaro *et al.*, *Phys. Rev. C* **88**, 054601 (2013).
- [11] D. Carbone *et al.*, *Phys. Rev. C* **95**, 034603 (2017).
- [12] J. L. Ferreira *et al.*, *Phys. Rev. C* **103**, 054604 (2021).
- [13] C. Kumar *et al.*, *Eur. Phys. J. A* **59**, 277 (2023).
- [14] <http://www.to.infn.it/~nanni/grazing>.
- [15] Ian J. Thompson, *Comput. Phys. Rep.* **7**, 167 (1988).
- [16] L. C. Chamon *et al.*, *Phys. Rev. C*, **66**, 014610 (2002).
- [17] N. Shimizu *et al.*, *Comput. Phys. Commun.* **244**, 372 (2019).
- [18] B. A. Brown *et al.*, *Phys. Rev. C* **71**, 044317 (2004).
- [19] R. Machleidt *et al.*, *Phys. Rev. C* **53**, R1483 (1996).
- [20] Chong Qi *et al.*, *Phys. Rev. C* **86**, 044323 (2012).
- [21] R. Banik *et al.*, *Phys. Rev. C* **101**, 014322 (2020).
- [22] T. Ishimatsu *et al.*, *Nucl. Phys. A* **104**, 481 (1967).
- [23] A. Poves *et al.*, *Nucl. Phys. A* **694**, 157 (2001).
- [24] W. A. Richter *et al.*, *Nucl. Phys. A* **523**, 325 (1991).
- [25] <http://www.fresco.org.uk>.
- [26] L. C. Chamon *et al.*, *Comput. Phys. Commun.* **267**, 108061 (2021).
- [27] A. Kundu *et al.*, *Phys. Rev. C* **99**, 034609 (2019).
- [28] O. Kenn *et al.*, *Phys. Rev. C* **63**, 064306 (2001).
- [29] A. G. Blair *et al.*, *Phys. Rev.* **151**, 930 (1966).
- [30] D. Montanari *et al.*, *Phys. Rev. C* **93**, 054623 (2016).